This is the peer reviewd version of the followng article:

Thermal conductivity of Li3PS4 solid electrolytes with ab initio accuracy / Tisi, Davide; Grasselli, Federico; Gigli, Lorenzo; Ceriotti, Michele. - In: PHYSICAL REVIEW MATERIALS. - ISSN 2475-9953. - 8:6(2024), pp. 065403-1-065403-11. [10.1103/PhysRevMaterials.8.065403]

Terms of use:

The terms and conditions for the reuse of this version of the manuscript are specified in the publishing policy. For all terms of use and more information see the publisher's website.

06/02/2025 14:33

(Article begins on next page)

Thermal conductivity of Li_3PS_4 solid electrolytes with *ab initio* accuracy

Davide Tisi,[1] Federico Grasselli,[1] Lorenzo Gigli,[1] and Michele Ceriotti[1, *]

[1]*Laboratory of Computational Science and Modeling, Institut des Matériaux,*
École Polytechnique Fédérale de Lausanne, 1015 Lausanne, Switzerland

(Dated: June 18, 2024)

The vast amount of computational studies on electrical conduction in solid-state electrolytes is not mirrored by comparable efforts addressing thermal conduction, which has been scarcely investigated despite its relevance to thermal management and (over)heating of batteries. The reason for this lies in the complexity of the calculations: on one hand, the diffusion of ionic charge carriers makes lattice methods formally unsuitable, due to the lack of equilibrium atomic positions needed for normal-mode expansion. On the other hand, the prohibitive cost of large-scale molecular dynamics (MD) simulations of heat transport in large systems at *ab initio* levels has hindered the use of MD-based methods. In this paper, we leverage recently developed machine-learning potentials targeting different *ab initio* functionals (PBEsol, r²SCAN, PBE0) and a state-of-the-art formulation of the Green-Kubo theory of heat transport in multicomponent systems to compute the thermal conductivity of a promising solid-state electrolyte, Li_3PS_4, in all its polymorphs (α, β, and γ). By comparing MD estimates with lattice methods on the low-temperature, nondiffusive γ-Li_3PS_4, we highlight strong anharmonicities and negligible nuclear quantum effects, hence further justifying MD-based methods even for nondiffusive phases. Finally, for the ion-conducting α and β phases, where the multicomponent Green-Kubo MD approach is mandatory, our simulations indicate a weak temperature dependence of the thermal conductivity, a glass-like behavior due to the effective local disorder characterizing these Li-diffusing phases.

I. INTRODUCTION

Thermal management is recognized as a major issue in both the design and practical manufacturing of modern batteries: insufficient or inhomogeneous thermal dissipation leads to overheating, particularly during rapid charging processes. Such overheating can, in turn, trigger severe events, like partial melting or explosions, or, more generally, degradation, non uniform charge conduction, and dendrite formation [1–3]. Given these circumstances, it is entirely justified to consider thermal runaway as "the key scientific problem in battery safety research" (verbatim from Ref. 4). Despite the need to study, in a quantitative way, the concurring mechanisms of heat dissipation (via ionic Joule effect) and charge flow at operating regimes, *thermal* transport in solid-state electrolytes (SSEs), which constitute the core of modern Li-ion batteries, has been only scarcely investigated, especially when compared to *charge* transport [5–16]. The interest in performing measurements of the thermal conductivity for several classes of SSEs has grown only very recently [17–19]. Computational studies, which are abundant for other classes of ionic materials [20–23], are even fewer than experimental ones and often rely on very crude models of microscopic thermal transport, which completely neglect the effects of vacancies, defects and, most importantly, ionic diffusion. This is due to the complexity of the calculations of thermal conductivity in SSEs: On the one hand, the absence of well-defined equilibrium atomic positions makes lattice methods—even when adapted to deal with disorder

and defects [24–27]—formally not suitable for SSEs, characterized by Li-ion diffusion occurring at the same time scale of heat transfer. On the other hand, although considerable theoretical efforts in the community have recently made *ab initio* simulations of heat transport from equilibrium molecular dynamics (MD) possible [28–31], the computational cost makes them impractical for large-scale simulations. In the last decade, the rise of machine-learning potential (MLPs) in combination with the Green-Kubo (GK) theory of linear response [32, 33] allowed the community to study the thermal properties of several complex and large systems [34–50].

In this paper, we address thermal conduction in a paradigmatic SSE, lithium ortho-thiophosphate (Li_3PS_4), a promising candidate for next-generation batteries thanks to the large ionic conductivity and wide electrochemical stability of its superionic polymorphs (the α and β phases) [6–13]. We leverage machine-learning potentials [51] and the extension of the GK theory of linear response to multicomponent systems [52] to compute the thermal conductivity κ of the different Li_3PS_4 polymorphs (i.e., the Li-ion diffusive α and β phases, as well as the nondiffusive γ phase) over a wide range of temperatures. The use of MLPs also allows us to compare estimates of κ from different target levels of density functional theory (DFT), namely the generalized-gradient-approximation (GGA) PBEsol [53, 54], the meta-GGA regularized SCAN (r²SCAN) [55] and the hybrid PBE0 [56] functionals.

---
* michele.ceriotti@epfl.ch

II. THEORY AND METHODS

A. Machine learning models

We use MLP models from our recent study on charge transport in Li$_3$PS$_4$ [51]: MLPs are constructed from kernel ridge regression, using the power spectrum of the smooth overlap of atomic positions (SOAP) [57] as features. The MLP model is built to fit the total potential energy E, and force components $\{\boldsymbol{F}_{i=1}^N\}$, where N is the number of atoms, over a training set of representative structures. Target properties are expressed as sums of local, atom-centered contributions predicted through kernel ridge regression,

$$E = \sum_{i \in A} \epsilon_i(A_i) = \sum_{i \in A} \sum_{j \in M} w_j \, \mathrm{k}(A_i, M_j) \tag{1}$$
$$\boldsymbol{F}_i = -\boldsymbol{\nabla}_i E$$

Here, A_i represents the environment surrounding atom i in structure A, $\epsilon_i(A_i)$ the potential energy associated with it, w_j are the weights to be optimized, and the kernel $\mathrm{k}(A_i, M_j)$ measures the correlation between the environment A_i and an environment M_j, taken from a representative set, the so-called sparse set M. We have used a quadratic kernel, $\mathrm{k}(A_i, A_j) = |\mathbf{p}_i \cdot \mathbf{p}_j|^2$, where $\mathbf{p}_i$ is the SOAP feature of the local environment A_i. Further details and specific hyperparameters of these Gaussian approximation potentials [58] can be found in the Supporting Information of Ref. [51]. Post-GGA models are trained using a two-level scheme [59, 60] whereby the difference with respect to a PBEsol ML baseline is learned on a representative subset of structures on which post-GGA calculations are performed. This learning strategy avoids running thousands of expensive post-GGA *ab initio* calculations while retaining good accuracy. Further details on data set generation and training details can be found in Ref. 51. Since thermal conduction is intertwined with the lattice elastic properties of a material, we have tested the reliability of our MLP in reproducing the bulk modulus of Li$_3$PS$_4$ via Murnaghan's equation of state (MEoS) [61–63] finding an agreement within 3 GPa, which is less than 10% of the typical values for this relatively soft material. See Supplemental Material (SM) [64], Sec. II, for details. In Sec. IV of the SM we discuss the phonon bands and vibrational density of states obtained with our MLP, finding good agreement with those computed *ab initio* within density functional perturbation theory [65].

B. Multicomponent Green-Kubo theory

Heat transport is quantified, in the linear response regime, by the thermal conductivity, κ, defined as the ratio between the heat flux and the negative temperature gradient in the absence of any convection. The GK theory of linear response [32, 33] provides a rigorous frame-

work to compute κ from equilibrium MD (EMD) simulations in terms of the stationary time series of properly defined microscopic fluxes sampled along the EMD trajectory. For one-component systems, solids and molecular fluids characterized by a single, nondissociated molecular type, the prescription of vanishing convection is trivially satisfied in MD simulations performed in the barycentric reference frame, since the center of mass of each atomic species does not diffuse. In particular, for an isotropic system of N interacting particles, the one-component GK expression reads:

$$\kappa = \frac{\Omega}{3k_{\mathrm{B}}T^2} \int_0^\infty \langle \boldsymbol{J}_e(\Gamma_t) \cdot \boldsymbol{J}_e(\Gamma_0) \rangle \, \mathrm{d}t, \tag{2}$$

where k_{B} is the Boltzmann constant, T the temperature and Γ_t indicates the evolution at time t of a point in phase space from the initial condition Γ_0, over which the equilibrium average $\langle \cdot \rangle$ is performed. The energy flux $\boldsymbol{J}_e$ is defined as [66]:

$$\boldsymbol{J}_e = \frac{1}{\Omega} \sum_{i=1}^N \left[e_i \boldsymbol{v}_i - \sum_{j=1}^N (\boldsymbol{r}_i - \boldsymbol{r}_j) \frac{\partial \epsilon_j}{\partial \boldsymbol{r}_i} \cdot \boldsymbol{v}_i \right] \tag{3}$$

where $\boldsymbol{r}_i$, $\boldsymbol{v}_i$ are the atomic positions and velocities, respectively; $e_i = \frac{1}{2}m_i v_i^2 + \epsilon_i$ is the atomic energy, sum of a kinetic contribution (m_i is the atomic mass) and a local potential energy term, ϵ_i. In the MLP picture, ϵ_i is given by the atomic partition of the potential energy of the ML model, as in Eq. (1) [50]. Recently, Langer *et al.* [44, 67] have also extended the definition of ML energy flux to semilocal, message-passing MLPs, and implemented it via automatic differentiation techniques.

Nevertheless, for a multicomponent system such as the conductive phases of Li$_3$PS$_4$, Eq. (2) cannot be applied as is: in fact, in a standard EMD simulation, keeping the center of mass of the entire system fixed does not imply that the centers of mass of each atomic species do not diffuse, and the prescription of vanishing convection is not satisfied [68]. Therefore, a theoretically justified and computationally robust method must be used to remove the coupling between the energy flux, $\boldsymbol{J}_e$ and the mass fluxes $\boldsymbol{J}_X = \frac{1}{\Omega} m_X \sum_{i \in X} \boldsymbol{v}_i$ of atomic species $X = $ Li, P, or S. A multivariate technique to do so was developed in Ref. 52: κ is estimated in terms of the zero-frequency limit of the so-called *reduced* power spectral density (PSD), i.e., the PSD $S_{ee}(\omega)$ of the energy flux that is obtained after removing its coupling to the mass fluxes:

$$\kappa = \lim_{\omega \to 0} \Lambda(\omega)$$
$$\Lambda(\omega) \equiv \frac{\Omega}{6k_{\mathrm{B}}T^2} \underbrace{[S_{ee}(\omega) - S_{\mathrm{coupl.}}(\omega)]}_{\text{reduced PSD}} \tag{4}$$

Here,

$$S_{\mathrm{coupl.}} \equiv \begin{pmatrix} S_{\mathrm{Li}e} & S_{\mathrm{P}e} \end{pmatrix} \begin{pmatrix} S_{\mathrm{LiLi}} & S_{\mathrm{LiP}} \\ S_{\mathrm{PLi}} & S_{\mathrm{PP}} \end{pmatrix}^{-1} \begin{pmatrix} S_{e\mathrm{Li}} \\ S_{e\mathrm{P}} \end{pmatrix} \tag{5}$$

and $S_{ab}(\omega) = \int_{-\infty}^{\infty} \langle \boldsymbol{J}_a(\Gamma_t) \cdot \boldsymbol{J}_b(\Gamma_0) \rangle e^{-i\omega t} \, dt$ is the cross-PSD between fluxes $\boldsymbol{J}_a$ and $\boldsymbol{J}_b$, with $a, b \in \{e, \text{Li}, \text{P}\}$ [69]. Notice that for solids and single-component systems, $\lim_{\omega \to 0} S_{\text{coupl.}} = 0$, and Eq. (4) reduces to Eq. (2), thanks to the Wiener-Khintchine theorem [70, 71]. See Refs. 72 and 73 for further details. An important remark is necessary: the partitioning of the total potential energy $E(A)$ into local contributions ϵ_i is not unique. In fact, two models that differ by a small change in the hyperparameters and/or training set, will lead to equivalent total energies and forces, but different ϵ_i. Nevertheless, GK theory still allows to uniquely define κ thanks to recently discovered *invariance principles* of transport coefficients, according to which κ is largely independent of the definition of microscopic energies [50, 73–75] This can be verified by explicit construction of a *committee* of MLPs via dataset subsampling [76], through which we can quantify how much local predictions are dependent on the model's details [77]. Such a model dependence of ϵ_i implies that different MLPs inevitably lead to different instantaneous values of the energy flux, $\boldsymbol{J}_e$, which is defined from local quantities. This is explicitly shown in Fig. 1 for a simulation of the α phase of Li_3PS_4 at $T = 650$ K, which is superionic and characterized by significant Li-ion diffusion. We consider a single EMD trajectory driven by a model (here labeled A) of a committee of MLPs obtained from subsampling the whole PBEsol dataset. We then compute the energy flux via Eq. (3), over this trajectory, for model A, as well as for other members of the same committee. We use the same trajectory to single out the role of model-dependent estimates of $\boldsymbol{J}_e$ from the effects due to sampling independent EMD trajectories, each run with a different member of the MLP committee. Despite the slight procedural abuse [78], this approach allows us to test the invariance principles of κ more directly. Figure 1 shows that different members of the committee give, on the same segment of trajectory, different estimates for $\boldsymbol{J}_e$ (panel a), as well as for the distribution of atomic energies per species (panel b). Nonetheless, the $\omega \to 0$ limit of the reduced PSD, here estimated via multivariate cepstral analysis [52, 79], is independent of the specific MLP committee member, as clearly shown in Fig. 1(c). An analogous analysis on more members of the committee gives the same result, see Fig. S5 within the SM [64]. It is worth remarking that whenever MLP models are trained for multicomponent systems with a fixed dataset stoichiometry, as in the case of Li_3PS_4, the average per-atom potential energies (and not only the shape of their distributions) is model dependent, see Fig. 1(b). This fact and the presence of diffusing species induce *model-dependent*, convective-like contributions to the heat flux that are responsible for different and incompatible values of $S_{ee}(0)$, as shown in the $\omega \to 0$ region of Fig. 2. Therefore, these values cannot be taken as meaningful estimates of κ, and are indeed several times larger than the correct value (black arrow), obtained from the multivariate formulation. Only the latter is able to remove the coupling of these convective
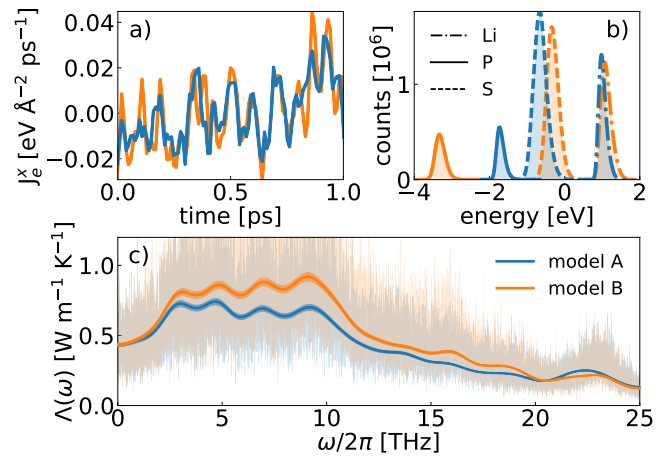

FIG. 1. Nonuniqueness of energy flux and invariance principles of thermal conductivity. (a) x Cartesian component of the energy flux $\boldsymbol{J}_e$ predicted, along a same segment of trajectory, by two models, here labeled A (blue) and B (orange), of a committee of PBEsol MLPs. (b) Distribution of atomic energies per species for the same two models over the same trajectory. Both shape and position differ between models A and B. (c) Reduced power spectra (pale, noisy background lines) and their cepstral filter (thick solid line with uncertainty) for models A and B. The values at $\omega \to 0$, representing the estimate of κ for models A and B, coincide. All results are obtained by recomputing the local energies and heat fluxes with models A and B on a trajectory generated by model A for the α phase equilibrated at $T = 650$ K and zero pressure.

contributions from heat conduction via the calculation of the *reduced* PSD.

The cepstral analysis of time series [79], employed to filter the noisy reduced PSD of Fig. 1(c) and Fig. 2, is a powerful filtering technique that has been already applied to estimate the thermal conductivity of complex materials [47, 80, 81], as well as other transport coefficients [82, 83]. We employ its implementation in the SPORTRAN code [84]. The calculation of $\boldsymbol{J}_e$, as shown in Eq. (3), consists of two terms: the first term depends only on e_i and the velocities and is trivial to compute; the second term depends on the so-called *atomic virial*, defined by

$$\text{W}_{i,\mu\nu} \equiv -\sum_j (r_{i,\mu} - r_{j,\mu}) \frac{\partial \epsilon_j}{\partial r_{i,\nu}} \qquad (6)$$

with $\mu, \nu \in \{x, y, z\}$. This is implemented in LIBRAS-CAL [85] by direct application of the chain rule to the SOAP features. Notice that, contrary to the total virial, the atomic virial need *not* be symmetric and all the nine Cartesian components must be stored to avoid miscalculations of κ (see Refs. [86, 87]). In particular, from the implementation standpoint, only pair potentials $v(|\boldsymbol{r}|)$ prescribe that $\text{W}_{i,\mu\nu} = \text{W}_{i,\nu\mu}$. In fact,

$$\frac{\partial v(|\boldsymbol{r}_{ij}|)}{\partial r_{i,\nu}} = \frac{\partial v(|\boldsymbol{r}_{ij}|)}{\partial r_{ji,\nu}} = \frac{1}{|\boldsymbol{r}_{ji}|} \frac{\partial v(|\boldsymbol{r}_{ij}|)}{\partial |\boldsymbol{r}_{ji}|} r_{ji,\nu}, \qquad (7)$$

where $\boldsymbol{r}_{ji} \equiv \boldsymbol{r}_i - \boldsymbol{r}_j$. Hence,

$$W_{i,\mu\nu} \propto \sum_j \frac{1}{|\boldsymbol{r}_{ji}|} r_{ji,\mu} \frac{\partial v(|\boldsymbol{r}_{ij}|)}{\partial |\boldsymbol{r}_{ji}|} r_{ji,\nu} \qquad (8)$$

is invariant under exchange of μ and ν. In the case of ML potentials with three-body descriptors, instead, we cannot assume that the atomic virials are symmetric, as already observed for general many-body potential [86–89]
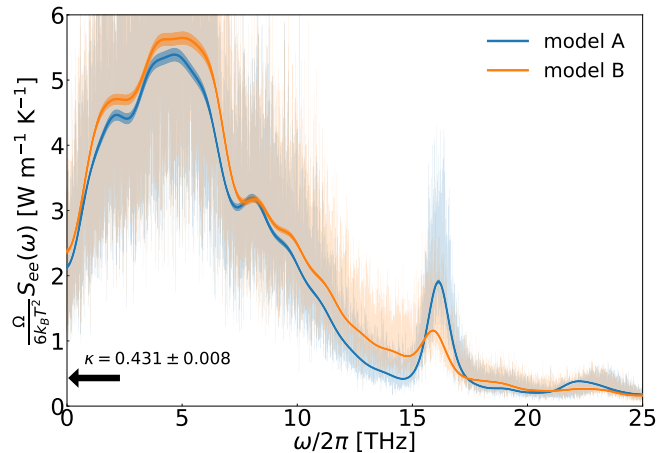

FIG. 2. Effect of incorrect use of $S_{ee}(\omega)$ instead of the full $\Lambda(\omega)$. $S_{ee}(0)$ not only depends on the ML model, but it is also very different from the correct value, taken from Fig. 1 and represented by the black arrow.

III. RESULTS

A. Validation of MD-based methods

The application of the multivariate Green-Kubo method via MD (GKMD) is necessary for phases and temperatures where the Li-ion diffusion prevents any expansion into normal modes due to the lack of well-defined equilibrium positions of the atoms. However, at temperatures that are sufficiently low to inhibit Li-ion diffusion, one might wonder whether lattice methods (LM), like the Boltzmann transport equation (BTE), would be more appropriate. LM are indeed more straightforward from a computational perspective: once the relevant interatomic force constants are computed, $\kappa(T)$ is available at any temperatures at very low computational cost; furthermore, LM do not require the long dynamics necessary to sufficiently sample the slow modes through GKMD. An example of the latter behavior of GKMD is presented in Fig. 3, which shows the heat-flux reduced PSD obtained via PBEsol-MLP on the γ phase at different temperatures and cell sizes. Resolving the narrow, steep peak at very low frequencies (< 0.1 THz) – that appears at $T = 200$ K and is absent at larger T – requires MD simulations of several nanoseconds and determines the larger
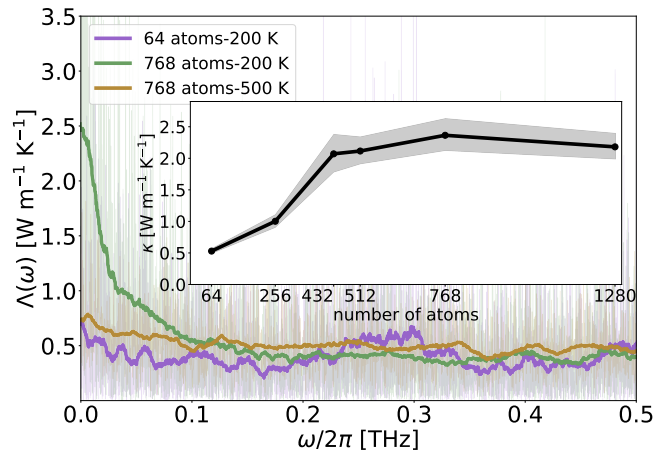

FIG. 3. Low-frequency portion of the heat-flux reduced PSD for the γ phase with 64-atom cell at $T = 200$ K (violet), 768-atom cell at $T = 200$ K (green) and 768-atom cell at 500 K (gold), filtered with a window of 0.025 THz. The curve for the system of 768 atoms at $T = 200$ K presents a steep peak (width ≈ 0.05 THz) at very low frequencies (< 0.1 THz).

uncertainty on κ for the γ phase at low temperature. Notice that such a low-frequency peak can only be captured using a large simulation cell, due to the long wavelength of the modes involved, as shown by comparison with the 64-atom system (a size-dependent estimate of κ and its uncertainty via cepstral analysis is shown in the inset to highlight finite-size effects). Lattice methods, instead, allow to interpolate the modes in the Brillouin zone, hence sampling at once both high and very low frequencies, provided a large enough supercell is used to converge interatomic force constants. Additionally, LM allow the inclusion of nuclear quantum effects (NQE) – that, in the presence of a light element such as lithium, cannot be *a priori* excluded [90], even at temperatures slightly above the Debye temperature, $T_D \approx 140$ K (see the SM [64] for details on the computations) – by simply considering quantum (Bose-Einstein) and classical (equipartition) occupations of the modes. However, the crucial drawback of LM is that, whenever the material is largely anharmonic, higher and higher orders of the normal-mode expansion should be computed and included in the calculation of κ. In addition, LM are technically applicable only when it is possible to define a minimum of the potential energy surface, which is the case only for the γ phase, but not for the β and α phases, and in general for any other SSEs that have equivalent unoccupied Wyckoff sites. The latter phases would in fact require several expensive LM calculations on very large systems – even in the absence of atomic diffusion – to correctly sample the effects of disorder in the Li-ion sub-lattice and obtain reliable values for κ.

In the following, we show that, due to the strong anharmonic effects of Li_3PS_4, and since NQE are shown to be largely negligible, GKMD has to be preferred with respect to LM even for the γ phase, at $T \gtrsim 200$ K. To
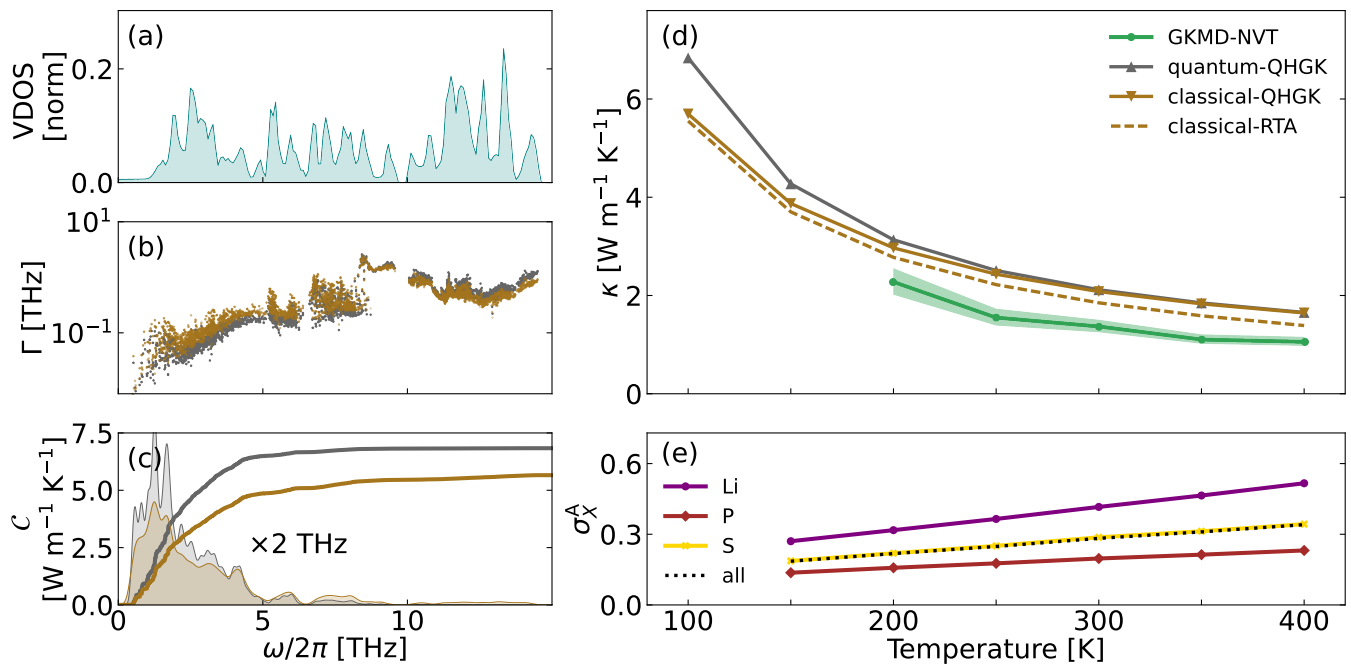
FIG. 4. Lattice-method approach to thermal conductivity of the γ phase at low T for the PBE0 model. Vibrational density of states (a), phonon linewidths (b), and cumulative integral of lattice thermal conductivity, with its density (c) for $T = 100$ K, for quantum (grey) and classical (brown) mode occupations. (d) $\kappa(T)$ via LM (on a $3 \times 3 \times 3$ supercell of the 16-atom primitive cell and $7 \times 7 \times 7$ interpolation) compared to the results from multicomponent GK theory for NVT EMD simulations. (e) Total and species-resolved degree of anharmonicity, Eq. (9), as function of T.

show this, we compute κ adopting LM with the recent formulations described in Refs. 24 and 25, which, besides recovering the BTE, are also able to account for effective corrections due to *interband* transitions between vibrational modes. To do so, we adopt the quasi-harmonic Green-Kubo (QHGK) formalism [24, 91], as implemented in κALDo [92].

Figure 4 shows LM results for PBE0 model, which displays the best overall accuracy against experiments for several physical observables [51]. The vibrational density of states (VDOS), Fig. 4(a), and the mode bandwidths Γ, plotted at $T = 200$ K in Fig. 4(b), are computed from finite differences using the LIBRASCAL-ASE calculator [85, 93], interfaced with κALDo. The per-mode contribution to the thermal conductivity, and its cumulative value, $\mathcal{C}(\omega)$, are shown in Fig. 4(c) for $T = 200$ K. We stress that $\mathcal{C}(\omega)$ stems from a modal representation of heat transport. Therefore it is must *not* be misinterpreted as an energy flux PSD: in fact, the lattice thermal conductivity can be either estimated in terms of the $\omega \to 0$ limit of the energy-flux PSD, or as the $\omega \to \infty$ limit of the cumulant function $\mathcal{C}(\omega)$. See SM [64] for further tests and computational details along with a study of the temperature dependence of the spectral decomposition of κ.

The results for $\kappa(T)$ for quantum and classical mode occupations are shown and compared with GKMD in Fig. 4(d). The increase in κ due to interband coupling [24, 25] is also highlighted by direct comparison

of the QHGK conductivity κ_{QHGK} with the single-mode relaxation-time approximation κ_{RTA}—which accounts for *intra*band relaxation only. Even the correction to RTA introduced by the inversion of the full scattering matrix in the BTE cannot be responsible for the difference between LM and MD results, since it amounts to less than 5% of the κ_{RTA}, as detailed in SM [64], Sec. VIII.

As it is often the case [47, 94], the thermal conductivity obtained via lattice methods is larger than that computed by GKMD, even when the classical distribution is employed, likely because of higher-order contributions to normal-mode scattering. To quantify the role of anharmonicity, since computing higher-order phonon scattering rate on the same supercell would be intractable, we employ the *degree of anharmonicity*,

$$\sigma_X^{\mathrm{A}} \equiv \sqrt{\frac{\sum_{i \in X} \sum_\mu \langle |F_{i,\mu}(\boldsymbol{R}) - F_{i,\mu}^{(2)}(\boldsymbol{R})|^2 \rangle}{\sum_{i \in X} \sum_\mu \langle |F_{i,\mu}(\boldsymbol{R})|^2 \rangle}} \quad (9)$$

introduced by Knoop *et al.* [95]. Here, $F_{i,\mu}(\boldsymbol{R})$ is the force acting on atom i along Cartesian component μ, a function of all atomic coordinates $\boldsymbol{R} \equiv (\boldsymbol{r}_1, \ldots, \boldsymbol{r}_N)$, and $F_{i,\mu}^{(2)}(\boldsymbol{R}) = -\sum_{j,\beta} \Phi_{i,\mu}^{j,\nu} \Delta r_{j,\nu}$ is its harmonic approximation, $\Phi_{i,\mu}^{j,\nu}$ being the set of force constants and $\Delta \boldsymbol{r}_j$ the deviation from equilibrium of atom j. σ_X^{A} is reported in Fig. 4(e) for different subsets of atoms $X = \mathrm{Li, P, S}$. The values are those typical of highly anharmonic materials like rocksalts, perovskites or chalcopyrites [23].

For the sake of comparison, at room temperature, silicon, a largely harmonic material, has significantly smaller $\sigma_{Si}^A \approx 0.15$ [95]. Both Li and S atomic vibrations are very anharmonic. The reason is quite intuitive for Li, as Li ions are prone to diffuse at larger T, while for S it is a consequence of the S librations that are a characteristic feature of Li_3PS_4. Overall, this analysis suggests that LM predict values of κ that are of the same order of magnitude than GKMD, yet consistently higher. Incorporating higher-order contributions to normal mode scattering, which generally reduce κ [47], might align LM predictions more closely with GKMD results.

B. Green-Kubo molecular dynamics

Having extensively justified, even at low T, the need for the GKMD method to calculate κ, we now discuss the results obtained for the thermal conductivity of the γ, β and α phases of Li_3PS_4 over a wide range of temperatures, for MLPs targeting PBEsol, r^2SCAN and PBE0 functionals. EMD simulations on 768-atom cells are run with i-PI [96] in the NpT ensemble, with stochastic velocity rescaling (SVR) thermostat [97] and a generalized Langevin barostat [98] on the cell volume to target zero pressure. In contrast with other types of thermostats, SVR is able to reproduce NVE results for dynamical properties featuring characteristic time scales of several picoseconds, such as the shear viscosity of water or the dynamic structure factor of a polymer chain in explicit water [99]. Furthermore, the SVR thermostat was recently shown to recover the results of GKMD thermal conductivity of simple superionic materials from NVE simulations, even at temperatures low enough to suppress ionic diffusion (see, e.g., the case of CaF_2 in Fig. S10 of the SM of Ref. 100). We have also verified that the barostat, with the chosen parameters, does not affect the statistical properties of correlation functions and GK estimates from NpT simulations, when compared to NVT (see the SM [64], Fig. S8). EMD trajectories are at least 2-ns long, and energy and mass fluxes are sampled every 10 fs, that is sufficient to avoid aliasing in the PSD. Imperfect ergodicity and the constraint on cell shape make simulations dependent on the phase in which the system is initialized. In Ref. 51, we have shown that simulations initialized in the nonconductive γ phase undergo a structural phase transition to a mixed α/β phase that is Li-ion conductive, whenever simulations are run beyond a critical temperature, T_c, that strongly depends on the DFT functional ($T_c \approx 625$ K for PBEsol, 750 K for PBE0, and 800 K for r^2SCAN). Experimentally, the γ-to-β transition (structural transition from symmetry group $Pmn2_1$ to $Pnma$) occurs at 573 K, while the transition to the α-phase ($Cmcm$ [101]) occurs at 746 K [7].

Figure 5 shows the results of the multicomponent cepstral analysis. Following previous studies of heat transport in ionic conductors [102, 103], we introduce two distinct heat-transport carriers, i.e. propagating and diffus-
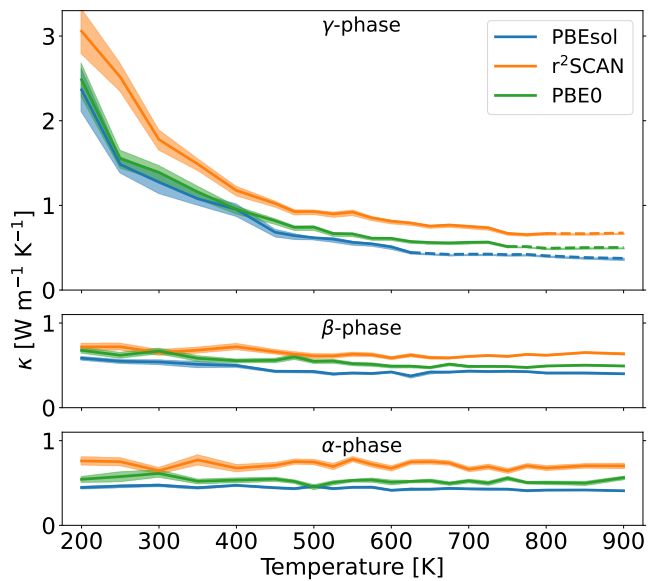

FIG. 5. Temperature behavior of the thermal conductivity of Li_3PS_4, $\kappa(T)$, for the γ, β and α phases and all the ML-models, from multicomponent Green-Kubo theory. Estimates (lines) and uncertainties (shaded areas) are obtained via multivariate cepstral analysis. The dashed lines in the top panel represent the regime where simulations, despite being initialized in the γ phase, undergo a transition to a mixed α/β phase, characterized by different ordering of PS_4 tetrahedra [51]. Notice the different vertical scale of top panel.

ing normal modes: propagating modes (also known as *propagons*), possess a nonvanishing group velocity and transport heat on a length scale usually larger than the interatomic distance via *intraband* scattering following conservation of total momentum. In contrast, diffusing modes (also known as *diffusons*) do not propagate and transport heat much more locally thanks to the *interband* coupling between different vibrational modes that are almost degenerate in energy and possess a finite lifetime. The simulations initialized in the γ phase (top panel) show a low-temperature crystal-like behavior, whereby κ decays with T, which is typical of heat transport mediated by phonon propagation. In contrast, simulations initialized in the β and α phases (mid and bottom panels, respectively) show an effective "glass-like" behavior [17] whereby κ is in practice independent of T: even at very low temperature, the disorder stemming from the large availability of empty Wyckoff sites for Li-ions in these phases (which promotes Li-diffusion at larger T) hinders phonon propagation in favor of diffusons, within the so-called Allen-Feldman regime [104], making these phases act like glasses, despite the overall crystalline arrangement of the PS_4 tetrahedra. Notice that the value of κ obtained from simulations initialized in the γ phase but equilibrated at $T > T_c$ matches the value obtained in simulations initialized in the α and β phases. The regime $T > T_c$ is represented by the dashed line in the top panel of Fig. 5.

For each T and phase, the largest values of κ are observed for r^{2}SCAN model, followed by PBE0, and finally by PBEsol. We have verified that the mere difference in the equilibrium volumes predicted by the different functionals cannot explain *per se* the significant difference between the estimates for κ (see the SM [64], Sec. VII). Interestingly, the largest *electrical* conductivities are instead found for PBEsol [51]: Li-ion diffusion affects the structure of the SSE by favoring disorder and inducing diffuson-like behavior typical of glass-like systems, even when the solid matrix (here composed by PS$_4$ tetrahedra) maintains crystalline order. The lower bulk modulus predicted for the γ phase by PBEsol (see the SM [64], Sec. II) also indicates softer bonding, usually promoting diffuson-like thermal transport [105]. Nevertheless, it would be improper, if not wrong, to speak of a quantitative relation between ionic and thermal conduction, especially on a local scale [102]. For instance, recent studies on argyrodites, another class of SSEs, highlight no significant correlation between the magnitude of ionic and thermal conductivity [103].

IV. CONCLUSIONS

Our thorough analysis of the nondiffusive, low-T γ phase shows that one must be very careful when using both lattice methods and molecular dynamics to study the thermal properties of SSEs: On one hand, lattice methods are not suited for systems with degrees of disorder, like those with empty Wyckoff sites where several equivalent minima of the potential energy surface are allowed. Moreover, the presence of large anharmonicity in Li$_3$PS$_4$ even at low T might make calculations up to three-phonon scattering not entirely reliable. On the other hand, MD-based methods need very long simulations to correctly sample the scattering of long-living, low-frequency phonons. Furthermore, large-scale simulations are needed, as finite-size effects tend to lower the estimate of κ with respect to converged values [100], making ML potentials essential for accurate simulations.

We also stress that MD-based calculations are in general tolerant to small inaccuracies of the force field (as long as the dynamics is correctly reproduced on average [106]), in contrast to lattice methods, where very accurate interatomic force constants are required. This feature further leans towards the use of GKMD, whenever ML potentials, usually trained on lower-order energy derivatives, are used and may not be able to reproduce high-order force constants, as shown for glasses in Ref. [48]. The use of GKMD to study these systems is also justified by the observation that nuclear quantum effects are negligible in the typical operating temperature regime (beyond 200 K) of SSEs. The use of MD also permits the study of other quantities crucial for the characterization of SSEs, such as the electrical conductivity, as well as conduction mechanisms. For instance, in Ref. [51], it has been shown that the ML-PBE0 model performs better than ML models targeting other *ab initio* functionals in predicting the charge-transport properties of Li$_3$PS$_4$.

Finally, in the Li-diffusive α and β phases of Li$_3$PS$_4$, the thermal conductivity is characterized by a glass-like behavior, with no significant dependence on the temperature nor on the specific phase, and values in line with recent experimental measures on amorphous lithium thiophosphates, i.e. in the range 0.45–0.70 W m^{-1} K^{-1} [17]: the crystalline arrangement of PS$_4$ groups is not sufficient to preserve the propagonic crystal-like behavior of $\kappa(T)$, which is hindered by the Li-ion disorder, induced by Li-ion diffusion and, even at low temperature, by the large availability of empty Wyckoff sites for Li ions, which are randomly arranged. Similarly, low values and a glass-like behavior of κ, indicating a prevalence of diffuson-like thermal transport, have also been found in experimental works on similar materials, such as Na$_3$PS$_4$ [107].

In summary, our study demonstrates that the combination of MLPs with GKMD is a promising approach for accurately calculating thermal conductivity at an *ab initio* level in lithium-based electrolytes. Large anharmonicity and ion diffusion make, in general, GKMD results more reliable than lattice methods for SSEs, once the multi-component analysis is correctly applied. This may be relevant for the prospective application to SSEs of high-throughput screening for thermal conductivity, that recently attracted great interest thanks to new semiautomated frameworks [23, 108, 109], in analogy to what has been pursued for the electrical conductivity [110–113] of SSEs. In particular, the possibility of computing the energy-flux time series in post processing also allows one to access thermal conductivity from the MD trajectories already produced to investigate the electrical conductivity which may be beneficial to jointly screen for both heat and charge transport of SSEs.

[1] Z. Rao, P. Lyu, P. Du, D. He, Y. Huo, and C. Liu, Thermal safety and thermal management of batteries, Battery Energy **1**, 20210019 (2022).

[2] A. K. Thakur, R. Sathyamurthy, R. Velraj, R. Saidur, A. Pandey, Z. Ma, P. Singh, S. K. Hazra, S. W. Sharshir, R. Prabakaran, *et al.*, A state-of-the art review on advancing battery thermal management systems for fast-charging, Appl. Therm. Eng. **226**, 120303 (2023).

[3] J. Wang, K. Yang, S. Sun, Q. Ma, G. Yi, X. Chen, Z. Wang, W. Yan, X. Liu, Q. Cai, *et al.*, Advances in thermal-related analysis techniques for solid-state lithium batteries, InfoMat **5**, e12401 (2023).

[4] X. Feng, M. Ouyang, X. Liu, L. Lu, Y. Xia, and X. He, Thermal runaway mechanism of lithium ion battery for electric vehicles: A review, Energy storage materials **10**, 246 (2018).

[5] V. Deshpande, C. Doerrer, M. Dyer, H. El-shinawi, N. Fleck, J. Irvine, H. Lee, G. Li, E. Liberti, I. Mcclelland, *et al.*, Roadmap on solid-state batteries, J. Phys. Energy **2**, 1088 (2020).

[6] Ömer Ulaş Kudu, T. Famprikis, S. Cretu, B. Porcheron, E. Salager, A. Demortiere, M. Courty, V. Viallet, T. L. Mercier, B. Fleutot, M.-D. Braida, and C. Masquelier, Structural details in Li_3PS_4: Variety in thiophosphate building blocks and correlation to ion transport, Energy Storage Materials **44**, 168 (2022).

[7] K. Homma, M. Yonemura, T. Kobayashi, M. Nagao, M. Hirayama, and R. Kanno, Crystal structure and phase transitions of the lithium ionic conductor Li_3PS_4, Solid State Ionics **182**, 53 (2011).

[8] T. Kimura, T. Inaoka, R. Izawa, T. Nakano, C. Hotehama, A. Sakuda, M. Tatsumisago, and A. Hayashi, Stabilizing high-temperature α-Li_3PS_4 by rapidly heating the glass, J. Am. Chem. Soc. **145**, 14466 (2023).

[9] N. J. de Klerk, E. van der Maas, and M. Wagemaker, Analysis of diffusion in solid-state electrolytes through md simulations, improvement of the Li-ion conductivity in β-Li_3PS_4 as an example, ACS applied energy materials **1**, 3230 (2018).

[10] F. N. Forrester, J. A. Quirk, T. Famprikis, and J. A. Dawson, Disentangling cation and anion dynamics in Li_3PS_4 solid electrolytes, Chemistry of Materials **34**, 10561 (2022).

[11] C. G. Staacke, H. H. Heenen, C. Scheurer, G. Csányi, K. Reuter, and J. T. Margraf, On the role of long-range electrostatics in machine-learned interatomic potentials for complex battery materials, ACS Applied Energy Materials **4**, 12562 (2021).

[12] C. G. Staacke, T. Huss, J. T. Margraf, K. Reuter, and C. Scheurer, Tackling structural complexity in Li2S-P2S5 solid-state electrolytes using machine learning potentials, Nanomaterials **12**, 2950 (2022).

[13] H. Guo, Q. Wang, A. Urban, and N. Artrith, Artificial Intelligence-Aided Mapping of the Structure–Composition–Conductivity Relationships of Glass–Ceramic Lithium Thiophosphate Electrolytes, Chemistry of Materials **34**, 6702 (2022), publisher: American Chemical Society.

[14] A. F. Harper, T. Huss, S. S. Köcher, and C. Scheurer, Tracking Li atoms in real-time with ultra-fast NMR simulations, ChemRxiv 10.26434/chemrxiv-2024-k4fbw (2024).

[15] T. Miyagawa, N. Krishnan, M. Grumet, C. R. Baecker, W. Kaiser, and D. A. Egger, Accurate description of ion migration in solid-state ion conductors from machine-learning molecular dynamics, J. Mater. Chem. A , (2024).

[16] R. Kobayashi, S. Takemoto, and R. Ito, Influence of nano-crystallization on Li-ion conductivity in glass Li_3PS_4: a molecular dynamics study, Journal of Solid State Electrochemistry 10.1007/s10008-024-05892-9 (2024).

[17] Z. Cheng, B. Zahiri, X. Ji, C. Chen, D. Chalise, P. V. Braun, and D. G. Cahill, Good solid-state electrolytes have low, glass-like thermal conductivity, Small **17**, 2101693 (2021).

[18] C.-W. Wu, X. Ren, W.-X. Zhou, G. Xie, and G. Zhang, Thermal stability and thermal conductivity of solid electrolytes, APL Materials **10**, 040902 (2022).

[19] T. Böger, T. Bernges, Y. Li, P. Canepa, and W. G. Zeier, Thermal conductivities of lithium-ion-conducting solid electrolytes, ACS Appl. Energy Mater. **6**, 10704 (2023).

[20] N. Ohtori, M. Salanne, and P. A. Madden, Calculations of the thermal conductivities of ionic materials by simulation with polarizable interaction potentials, The Journal of Chemical Physics **130**, 104507 (2009).

[21] H. Kim, S. Ballikaya, H. Chi, J.-P. Ahn, K. Ahn, C. Uher, and M. Kaviany, Ultralow thermal conductivity of β-Cu_2Se by atomic fluidity and structure distortion, Acta Materialia **86**, 247 (2015).

[22] Y. Zhou, S. Xiong, X. Zhang, S. Volz, and M. Hu, Thermal transport crossover from crystalline to partial-crystalline partial-liquid state, Nature Communications **9**, 4712 (2018).

[23] F. Knoop, T. A. R. Purcell, M. Scheffler, and C. Carbogno, Anharmonicity in thermal insulators: An analysis from first principles, Phys. Rev. Lett. **130**, 236301

(2023).

[24] L. Isaeva, G. Barbalinardo, D. Donadio, and S. Baroni, Modeling heat transport in crystals and glasses from a unified lattice-dynamical approach, Nat. Commun. **10**, 3853 (2019).

[25] M. Simoncelli, N. Marzari, and F. Mauri, Unified theory of thermal transport in crystals and glasses, Nat. Phys. **15**, 809 (2019).

[26] G. Caldarelli, M. Simoncelli, N. Marzari, F. Mauri, and L. Benfatto, Many-body Green's function approach to lattice thermal transport, Phys. Rev. B **106**, 024312 (2022).

[27] A. Fiorentino and S. Baroni, From Green-Kubo to the full Boltzmann kinetic approach to heat transport in crystals and glasses, Phys. Rev. B **107**, 054311 (2023).

[28] A. Marcolongo, P. Umari, and S. Baroni, Microscopic theory and quantum simulation of atomic heat transport, Nature Physics **12**, 80 (2016).

[29] A. Marcolongo, R. Bertossa, D. Tisi, and S. Baroni, QEHeat: An open-source energy flux calculator for the computation of heat-transport coefficients from first principles, Computer Physics Communications **269**, 108090 (2021).

[30] J. Kang and L.-W. Wang, First-principles Green-Kubo method for thermal conductivity calculations, Phys. Rev. B **96**, 020302 (2017).

[31] C. Carbogno, R. Ramprasad, and M. Scheffler, Ab Initio Green-Kubo Approach for the Thermal Conductivity of Solids, Phys. Rev. Lett. **118**, 175901 (2017).

[32] M. S. Green, Markoff random processes and the statistical mechanics of time-dependent phenomena, II. Irreversible processes in fluids, J. Chem. Phys. **22**, 398 (1954).

[33] R. Kubo, Statistical-mechanical theory of irreversible processes. I. General Theory and Simple Applications to Magnetic and Conduction Problems, J. Phys. Soc. Jpn. **12**, 570 (1957).

[34] G. C. Sosso, D. Donadio, S. Caravati, J. Behler, and M. Bernasconi, Thermal transport in phase-change materials from atomistic simulations, Phys. Rev. B **86**, 104301 (2012).

[35] P. Korotaev, I. Novoselov, A. Yanilkin, and A. Shapeev, Accessing thermal conductivity of complex compounds by machine learning interatomic potentials, Phys. Rev. B **100**, 144308 (2019).

[36] X. Qian, S. Peng, X. Li, Y. Wei, and R. Yang, Thermal conductivity modeling using machine learning potentials: application to crystalline and amorphous silicon, Materials Today Physics **10**, 100140 (2019).

[37] R. Li, Z. Liu, A. Rohskopf, K. Gordiz, A. Henry, E. Lee, and T. Luo, A deep neural network interatomic potential for studying thermal conductivity of β-Ga$_2$O$_3$, Applied Physics Letters **117**, 152102 (2020).

[38] K. Shimamura, Y. Takeshita, S. Fukushima, A. Koura, and F. Shimojo, Computational and training requirements for interatomic potential based on artificial neural network for estimating low thermal conductivity of silver chalcogenides, The Journal of Chemical Physics **153**, 234301 (2020).

[39] R. Li, E. Lee, and T. Luo, A unified deep neural network potential capable of predicting thermal conductivity of silicon in different phases, Materials Today Physics **12**, 100181 (2020).

[40] C. Mangold, S. Chen, G. Barbalinardo, J. Behler, P. Pochet, K. Termentzidis, Y. Han, L. Chaput, D. Lacroix, and D. Donadio, Transferability of neural network potentials for varying stoichiometry: Phonons and thermal conductivity of Mn$_x$Ge$_y$ compounds, Journal of Applied Physics **127**, 244901 (2020).

[41] H. Liu, X. Qian, H. Bao, C. Y. Zhao, and X. Gu, High-temperature phonon transport properties of SnSe from machine-learning interatomic potential, Journal of Physics: Condensed Matter **33**, 405401 (2021).

[42] Z. Fan, Z. Zeng, C. Zhang, Y. Wang, K. Song, H. Dong, Y. Chen, and T. Ala-Nissila, Neuroevolution machine learning potentials: Combining high accuracy and low cost in atomistic simulations and application to heat transport, Phys. Rev. B **104**, 104309 (2021).

[43] C. Verdi, F. Karsai, P. Liu, R. Jinnouchi, and G. Kresse, Thermal transport and phase transitions of zirconia by on-the-fly machine-learned interatomic potentials, npj Computational Materials **7**, 156 (2021).

[44] M. F. Langer, F. Knoop, C. Carbogno, M. Scheffler, and M. Rupp, Heat flux for semilocal machine-learning potentials, Phys. Rev. B **108**, L100302 (2023).

[45] K. Xu, Y. Hao, T. Liang, P. Ying, J. Xu, J. Wu, and Z. Fan, Accurate prediction of heat conductivity of water by a neuroevolution potential, The Journal of Chemical Physics **158**, 204114 (2023).

[46] Z. Sun, Z. Qi, K. Liang, X. Sun, Z. Zhang, L. Li, Q. Wang, G. Zhang, G. Wu, and W. Shen, A neuroevolution potential for predicting the thermal conductivity of α, β, and ϵ-Ga$_2$O$_3$, Applied Physics Letters **123**, 192202 (2023).

[47] P. Pegolo, S. Baroni, and F. Grasselli, Temperature-and vacancy-concentration-dependence of heat transport in Li$_3$ClO from multi-method numerical simulations, npj Comput. Mater. **8**, 24 (2022).

[48] P. Pegolo and F. Grasselli, Thermal transport of glasses via machine learning driven simulations, Frontiers in Materials **11**, 10.3389/fmats.2024.1369034 (2024).

[49] H. Dong, Y. Shi, P. Ying, K. Xu, T. Liang, Y. Wang, Z. Zeng, X. Wu, W. Zhou, S. Xiong, S. Chen, and Z. Fan, Molecular dynamics simulations of heat transport using machine-learned potentials: A mini-review and tutorial on GPUMD with neuroevolution potentials, Journal of Applied Physics **135**, 161101 (2024).

[50] D. Tisi, L. Zhang, R. Bertossa, H. Wang, R. Car, and S. Baroni, Heat transport in liquid water from first-principles and deep neural network simulations, Phys. Rev. B **104**, 224202 (2021).

[51] L. Gigli, D. Tisi, F. Grasselli, and M. Ceriotti, Mechanism of charge transport in lithium thiophosphate, Chemistry of Materials **36**, 1482 (2024).

[52] R. Bertossa, F. Grasselli, L. Ercole, and S. Baroni, Theory and numerical simulation of heat transport in multicomponent systems, Phys. Rev. Lett. **122**, 255901 (2019).

[53] J. P. Perdew, K. Burke, and M. Ernzerhof, Generalized gradient approximation made simple, Phys. Rev. Lett. **77**, 3865 (1996).

[54] J. P. Perdew, A. Ruzsinszky, G. I. Csonka, O. A. Vydrov, G. E. Scuseria, L. A. Constantin, X. Zhou, and K. Burke, Restoring the density-gradient expansion for exchange in solids and surfaces, Phys. Rev. Lett. **100**, 136406 (2008).

[55] J. W. Furness, A. D. Kaplan, J. Ning, J. P. Perdew, and J. Sun, Accurate and numerically efficient r2SCAN

meta-generalized gradient approximation, J. Phys. Chem. Lett. **11**, 8208 (2020).

[56] C. Adamo and V. Barone, Toward reliable density functional methods without adjustable parameters: The PBE0 model, J. Chem. Phys. **110**, 6158 (1999).

[57] A. P. Bartók, R. Kondor, and G. Csányi, On representing chemical environments, Phys. Rev. B **87**, 184115 (2013).

[58] A. P. Bartók, M. C. Payne, R. Kondor, and G. Csányi, Gaussian Approximation Potentials: The Accuracy of Quantum Mechanics, without the Electrons, Physical Review Letters **104**, 136403 (2010), arXiv:0910.1019.

[59] R. Ramakrishnan, P. O. Dral, M. Rupp, and O. A. von Lilienfeld, Big data meets quantum chemistry approximations: The δ-machine learning approach, Journal of Chemical Theory and Computation **11**, 2087 (2015).

[60] P. Zaspel, B. Huang, H. Harbrecht, and O. A. von Lilienfeld, Boosting quantum machine learning models with a multilevel combination technique: Pople diagrams revisited, Journal of Chemical Theory and Computation **15**, 1546 (2019).

[61] F. D. Murnaghan, Finite deformations of an elastic solid, American Journal of Mathematics **59**, 235 (1937).

[62] F. D. Murnaghan, The compressibility of media under extreme pressures, Proceedings of the National Academy of Sciences **30**, 244 (1944).

[63] F. Birch, Finite elastic strain of cubic crystals, Phys. Rev. **71**, 809 (1947).

[64] See Supplemental Material (ancillary file), which contains additional Refs. 116–121, for additional tests of the ML models and further details on invariance principles and lattice methods.

[65] S. Baroni, S. de Gironcoli, A. Dal Corso, and P. Giannozzi, Phonons and related crystal properties from density-functional perturbation theory, Rev. Mod. Phys. **73**, 515 (2001).

[66] J. H. Irving and J. G. Kirkwood, The Statistical Mechanical Theory of Transport Processes. IV. The Equations of Hydrodynamics, The Journal of Chemical Physics **18**, 817 (2004).

[67] M. F. Langer, J. T. Frank, and F. Knoop, Stress and heat flux via automatic differentiation, The Journal of Chemical Physics **159**, 174105 (2023).

[68] P. Lindan and M. Gillan, A molecular dynamics study of the thermal conductivity of CaF_2 and UO_2, Journal of Physics: Condensed Matter **3**, 3929 (1991).

[69] The mass flux of sulfur atoms does not appear explicitly, as it can be expressed in terms of $\boldsymbol{J}_{Li}$ and $\boldsymbol{J}_P$, because of total momentum conservation.

[70] N. Wiener, Generalized harmonic analysis, Acta mathematica **55**, 117 (1930).

[71] A. Khintchine, Korrelationstheorie der stationären stochastischen Prozesse, Math. Ann. **109**, 604 (1934).

[72] S. Baroni, R. Bertossa, L. Ercole, F. Grasselli, and A. Marcolongo, Heat transport in insulators from ab initio green-kubo theory, Handbook of materials modeling: Applications: Current and emerging materials (Springer Cham). Chap. **12**, 809 (2020).

[73] F. Grasselli and S. Baroni, Invariance principles in the theory and computation of transport coefficients, European Physical Journal B **94**, 160 (2021), 2105.02137.

[74] A. Marcolongo, L. Ercole, and S. Baroni, Gauge fixing for heat-transport simulations, Journal of Chemical Theory and Computation **16**, 3352 (2020).

[75] L. Ercole, A. Marcolongo, P. Umari, and S. Baroni, Gauge Invariance of Thermal Transport Coefficients, Journal of Low Temperature Physics **185**, 79 (2016).

[76] F. Musil, M. J. Willatt, M. A. Langovoy, and M. Ceriotti, Fast and Accurate Uncertainty Estimation in Chemical Machine Learning, Journal of Chemical Theory and Computation **15**, 906 (2019), publisher: American Chemical Society.

[77] S. Chong, F. Grasselli, C. Ben Mahmoud, J. D. Morrow, V. L. Deringer, and M. Ceriotti, Robustness of local predictions in atomistic machine learning models, Journal of Chemical Theory and Computation **19**, 8020 (2023).

[78] Equation (3) is obtained by enforcing Newton's second law, hence the use of a single trajectory is justified only when the spread in the forces predicted by the committee members vanishes.

[79] L. Ercole, A. Marcolongo, and S. Baroni, Accurate thermal conductivities from optimally short molecular dynamics simulations, Scientific reports **7**, 15835 (2017).

[80] F. Grasselli, L. Stixrude, and S. Baroni, Heat and charge transport in H_2O at ice-giant conditions from ab initio molecular dynamics simulations, Nature Communications **11**, 3605 (2020).

[81] L. Pan, J. Carrete, Z. Wang, and G. K. H. Madsen, Machine learning boosted *ab initio* study of the thermal conductivity of Janus PtSTe van der Waals heterostructures, Phys. Rev. B **109**, 035417 (2024).

[82] C. Malosso, L. Zhang, R. Car, S. Baroni, and D. Tisi, Viscosity in water from first-principles and deep-neural-network simulations, npj Comput. Mater. **8**, 139 (2022).

[83] P. Pegolo, S. Baroni, and F. Grasselli, Self-interaction and transport of solvated electrons in molten salts, The Journal of Chemical Physics **159**, 094116 (2023).

[84] L. Ercole, R. Bertossa, S. Bisacchi, and S. Baroni, SporTran: A code to estimate transport coefficients from the cepstral analysis of (multivariate) current time series, Computer Physics Communications **280**, 108470 (2022).

[85] F. Musil, M. Veit, A. Goscinski, G. Fraux, M. J. Willatt, M. Stricker, T. Junge, and M. Ceriotti, Efficient implementation of atom-density representations, The Journal of Chemical Physics **154**, 114109 (2021).

[86] Z. Fan, L. F. C. Pereira, H.-Q. Wang, J.-C. Zheng, D. Donadio, and A. Harju, Force and heat current formulas for many-body potentials in molecular dynamics simulations with applications to thermal conductivity calculations, Physical Review B **92**, 094301 (2015).

[87] D. Surblys, H. Matsubara, G. Kikugawa, and T. Ohara, Application of atomic stress to compute heat flux via molecular dynamics for systems with many-body interactions, Phys. Rev. E **99**, 051301 (2019).

[88] P. Boone, H. Babaei, and C. E. Wilmer, Heat Flux for Many-Body Interactions: Corrections to LAMMPS, Journal of Chemical Theory and Computation **15**, 5579 (2019).

[89] D. Surblys, H. Matsubara, G. Kikugawa, and T. Ohara, Methodology and meaning of computing heat flux via atomic stress in systems with constraint dynamics, Journal of Applied Physics **130**, 215104 (2021).

[90] M. Ceriotti, G. Miceli, A. Pietropaolo, D. Colognesi, A. Nale, M. Catti, M. Bernasconi, and M. Parrinello, Nuclear quantum effects in ab initio dynamics: Theory and experiments for lithium imide, Phys. Rev. B **82**, 174306 (2010).

[91] Reference 27 shows that QHGK is equivalent to the Wigner transport equation formulated in Refs. 25 and 26.

[92] G. Barbalinardo, Z. Chen, N. W. Lundgren, and D. Donadio, Efficient anharmonic lattice dynamics calculations of thermal transport in crystalline and disordered solids, J. Appl. Phys. **128**, 135104 (2020).

[93] A. H. Larsen, J. J. Mortensen, J. Blomqvist, I. E. Castelli, R. Christensen, M. Dułak, J. Friis, M. N. Groves, B. Hammer, C. Hargus, *et al.*, The atomic simulation environment—a Python library for working with atoms, J. Phys.: Condens. Matter **29**, 273002 (2017).

[94] M. Puligheddu, Y. Xia, M. Chan, and G. Galli, Computational prediction of lattice thermal conductivity: A comparison of molecular dynamics and Boltzmann transport approaches, Phys. Rev. Mater. **3**, 085401 (2019).

[95] F. Knoop, T. A. Purcell, M. Scheffler, and C. Carbogno, Anharmonicity measure for materials, Physical Review Materials **4**, 083809 (2020).

[96] V. Kapil, M. Rossi, O. Marsalek, R. Petraglia, Y. Litman, T. Spura, B. Cheng, A. Cuzzocrea, R. H. Meißner, D. M. Wilkins, *et al.*, i-pi 2.0: A universal force engine for advanced molecular simulations, Computer Physics Communications **236**, 214 (2019).

[97] G. Bussi, D. Donadio, and M. Parrinello, Canonical sampling through velocity rescaling, J. Chem. Phys. **126**, 14101 (2007).

[98] M. Ceriotti, G. Bussi, and M. Parrinello, Langevin Equation with Colored Noise for Constant-Temperature Molecular Dynamics Simulations, Phys. Rev. Lett. **102**, 020601 (2009).

[99] J. E. Basconi and M. R. Shirts, Effects of temperature control algorithms on transport properties and kinetics in molecular dynamics simulations, Journal of chemical theory and computation **9**, 2887 (2013).

[100] F. Grasselli, Investigating finite-size effects in molecular dynamics simulations of ion diffusion, heat transport, and thermal motion in superionic materials, The Journal of Chemical Physics **156**, 134705 (2022).

[101] K. Kaup, L. Zhou, A. Huq, and L. F. Nazar, Impact of the Li substructure on the diffusion pathways in alpha and beta Li_3PS_4: an in situ high temperature neutron diffraction study, Journal of Materials Chemistry A **8**, 12446 (2020).

[102] M. T. Agne, T. Böger, T. Bernges, and W. G. Zeier, Importance of thermal transport for the design of solid-state battery materials, PRX Energy **1**, 031002 (2022).

[103] T. Bernges, R. Hanus, B. Wankmiller, K. Imasato, S. Lin, M. Ghidiu, M. Gerlitz, M. Peterlechner, S. Graham, G. Hautier, *et al.*, Considering the role of ion transport in diffuson-dominated thermal conductivity, Advanced Energy Materials **12**, 2200717 (2022).

[104] P. B. Allen and J. L. Feldman, Thermal conductivity of disordered harmonic solids, Phys. Rev. B **48**, 12581 (1993).

[105] R. Hanus, M. T. Agne, A. J. Rettie, Z. Chen, G. Tan, D. Y. Chung, M. G. Kanatzidis, Y. Pei, P. W. Voorhees, and G. J. Snyder, Lattice softening significantly reduces thermal conductivity and leads to high thermoelectric efficiency, Advanced Materials **31**, 1900108 (2019).

[106] G. Pastore, E. Smargiassi, and F. Buda, Theory of ab initio molecular-dynamics calculations, Phys. Rev. A **44**, 6334 (1991).

[107] T. Bernges, T. Böger, O. Maus, P. S. Till, M. T. Agne, and W. G. Zeier, Scaling Relations for Ionic and Thermal Transport in the Na^+ Ionic Conductor Na_3PS_4, ACS Materials Letters **4**, 2491 (2022).

[108] F. Knoop, M. Scheffler, and C. Carbogno, Ab initio Green-Kubo simulations of heat transport in solids: Method and implementation, Phys. Rev. B **107**, 224304 (2023).

[109] M. Islamov, H. Babaei, R. Anderson, K. B. Sezginel, J. R. Long, A. J. H. McGaughey, D. A. Gomez-Gualdron, and C. E. Wilmer, High-throughput screening of hypothetical metal-organic frameworks for thermal conductivity, npj Computational Materials **9**, 11 (2023).

[110] A. D. Sendek, Q. Yang, E. D. Cubuk, K.-A. N. Duerloo, Y. Cui, and E. J. Reed, Holistic computational structure screening of more than 12000 candidates for solid lithium-ion conductor materials, Energy & Environmental Science **10**, 306 (2017).

[111] S. Muy, J. Voss, R. Schlem, R. Koerver, S. J. Sedlmaier, F. Maglia, P. Lamp, W. G. Zeier, and Y. Shao-Horn, High-throughput screening of solid-state Li-ion conductors using lattice-dynamics descriptors, Iscience **16**, 270 (2019).

[112] B. He, S. Chi, A. Ye, P. Mi, L. Zhang, B. Pu, Z. Zou, Y. Ran, Q. Zhao, D. Wang, *et al.*, High-throughput screening platform for solid electrolytes combining hierarchical ion-transport prediction algorithms, Scientific Data **7**, 151 (2020).

[113] L. Kahle, A. Marcolongo, and N. Marzari, High-throughput computational screening for solid-state Li-ion conductors, Energy & Environmental Science **13**, 928 (2020).

[114] L. Talirz, S. Kumbhar, E. Passaro, A. V. Yakutovich, V. Granata, F. Gargiulo, M. Borelli, M. Uhrin, S. P. Huber, S. Zoupanos, *et al.*, Materials Cloud, a platform for open computational science, Scientific data **7**, 1 (2020).

[115] European Organization For Nuclear Research and OpenAIRE, Zenodo (2013).

[116] Z. Deng, Z. Wang, I.-H. Chu, J. Luo, and S. P. Ong, Elastic properties of alkali superionic conductor electrolytes from first principles calculations, Journal of The Electrochemical Society **163**, A67 (2015).

[117] G. Materzanini, T. Chiarotti, and N. Marzari, Solids that are also liquids: elastic tensors of superionic materials, npj Computational Materials **9**, 10 (2023).

[118] Q. Chen and B. Sundman, Calculation of debye temperature for crystalline structures—a case study on Ti, Zr, and Hf, Acta Materialia **49**, 947 (2001).

[119] V. L. Moruzzi, J. F. Janak, and K. Schwarz, Calculated thermal properties of metals, Phys. Rev. B **37**, 790 (1988).

[120] O. L. Anderson, A simplified method for calculating the Debye temperature from elastic constants, Journal of Physics and Chemistry of Solids **24**, 909 (1963).

[121] O. L. Anderson, Determination and some uses of isotropic elastic constants of polycrystalline aggregates using single crystal data., in *Physical Acoustics*, Vol. III, Part B, edited by W. P. Mason (Academic Press, New York, 1965) p. 43.